PHYSICAL REVIEW B **78**, 214108 (2008)

Binding-energy relations and equations of state for the 4*d* and 5*d* transition metals

T. Qin,[1,*] R. Drautz,[1,2] and D. G. Pettifor[1]
[1]*Department of Materials, University of Oxford, Parks Road, Oxford OX1 3PH, United Kingdom*
[2]*ICAMS, Ruhr-Universität Bochum, 44780 Bochum, Germany*
(Received 21 August 2008; published 22 December 2008)

A recently proposed six-parameter mixed power-exponential expression is tested against density-functional theory binding-energy curves and equations of state across the 4*d* and 5*d* transition-metal series. It is shown to remove known failures of the popular Birch-Murnaghan, extended Rydberg, and generalized Morse expressions in that it is able to not only reproduce the observed hard-core repulsion of the early transition metals under compression but also remove predicted spurious oscillations in the binding-energy relations under expansion. However, it is unable to fit the well-known anomalous behavior of the equation of state for lanthanum.

DOI: 10.1103/PhysRevB.78.214108 PACS number(s): 64.30.Ef, 62.50.−p, 71.15.Nc, 71.20.Be

I. INTRODUCTION

Many different analytic binding-energy relations (BERs) and equations of state have been proposed for fitting both experimental data and first-principles quantum-mechanical calculations. A reliable *binding-energy relation* of the energy versus volume enables one to understand the cohesion of materials. Thus, it can assist theorists in the construction of interatomic potentials such as in the embedded-atom method.[1–3] However, shortcomings in the parametrization of the binding-energy relation at high pressures can generate unreliable predictions from molecular-dynamics simulations of collision cascades under radiation damage,[4] for example. An accurate *equation of state* (EOS) of the pressure versus volume enables experimentalists to parametrize experimental data and gain physical insight. For example, analytic equations of states have been extensively used by geophysicists to extrapolate the pressure to the earth's core and study its properties.[5]

In this paper we will begin by examining the three most commonly used analytic forms, namely, the Birch-Murnaghan,[6,7] the extended Rydberg,[8,9] and the generalized Morse,[10,11] respectively. The first was proposed in 1952, expressing the energy of a bulk material as an expansion in powers of the strain that results from either a uniform compression or expansion. The second is an extension of the interatomic potential proposed by Rydberg in 1932 for modeling the vibrational spectra of diatomic molecules. It found great popularity 20 years ago when Rose *et al.*[12] and Vinet *et al.*[13] reintroduced it as a universal binding-energy relation and equation of state, respectively. The third is a generalization of the exponential-type interatomic potential that had originally been proposed by Morse in 1929 for modeling vibrational spectra of dimers and subsequently was successfully applied by Slater[14] and Ducastelle[11] to model covalent materials and transition metals. During subsequent years many authors have addressed the failures of these expressions. In particular, under high pressure the Birch-Murnaghan equation of state can become unstable,[15–17] and the extended Rydberg expansion and generalized Morse expression do not provide sufficient hard-core repulsion.[18–21]

In this paper we will show how to go beyond these limitations. The analytic forms of the binding-energy relations and equations of state will be tested systematically across the 4*d* and 5*d* transition-metal series. First, the failures within the binding-energy relations based on the Birch-Murnaghan, extended Rydberg, and generalized Morse expressions will be analyzed and discussed in Sec. II. The corresponding failures in the equations of state will be discussed in Sec. III. In Sec. IV an improved expression, which we proposed recently to remedy these failures,[22] will be discussed and tested across the 4*d* and 5*d* transition-metal series. In Sec. V we conclude.

II. BINDING-ENERGY RELATIONS

The analytic binding-energy relations are usually fitted to known values of the cohesive energy E_0, equilibrium volume V_0, bulk modulus K_0, and pressure derivatives of the bulk modulus such as K_0'. In order to perform a detailed analysis of the applications of different forms of binding-energy relations to the 4*d* and 5*d* transition metals, we have chosen to generate a consistent high-quality database of binding-energy curves by using density-functional theory (DFT). We have used the Vienna *ab initio* simulation package (VASP) (Refs. 23 and 24) with projected augmented wave (PAW) (Ref. 25) method. The calculations are run within the local-density approximation (LDA) (Ref. 26) to the exchange-correlation functional except for Lu where the Perdew-Burke-Ernzerhof (PBE) (Ref. 27) approximation is used since only PBE is provided in VASP for Lu. In order to obtain accurate data at high pressures, the semicore electrons are treated as valence electrons[28] and a large cut-off energy of 430 eV is taken. The Brillouin-zone sampling is performed using the Monkhorst-Pack scheme[29] and the **k**-point mesh is chosen as $(45/2\pi)$ times the length of the reciprocal vector (e.g., $15\times15\times9$ is used for hcp Lu at equilibrium). The binding energy and pressure are calculated for all three common metallic structure-types bcc, fcc, and hcp (with c/a fixed as the equilibrium value).

The values of the predicted DFT ground-state cohesive energy, equilibrium volume, bulk modulus, and its first-order pressure derivative are shown in Fig. 1 for the 4*d* and 5*d* transition-metal series. We have obtained E_0, V_0, and K_0 by

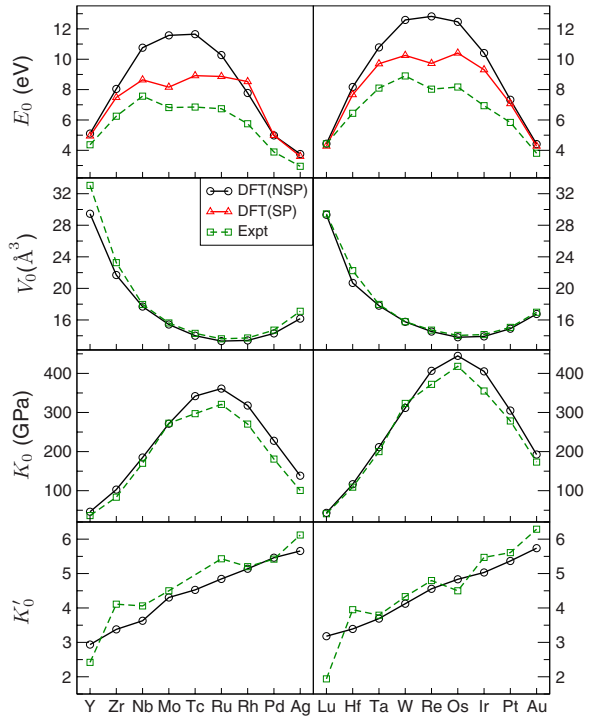

FIG. 1. (Color online) Comparison of DFT and experimental values (Refs. 32–35) of E_0, V_0, K_0 and K_0' across the $4d$ (left-hand panel) and $5d$ (right-hand panel) transition-metal series. Values of E_0 calculated with respect to NSP and SP free-atom energies are given by solid lines connected by circles and triangles, respectively.

using polynomial fitting around equilibrium over the range $|V^{1/3}-V_0^{1/3}|/V_0^{1/3} \leq 5\%$, whereas K_0' is obtained using the procedure described in Ref. 22 and in Sec. IV. We see that the DFT results are consistent with the experimental data. As is well-known non-spin-polarized (NSP) DFT calculations overestimate the cohesive energy by about 4 eV due to the neglect of the spin polarization of the free-atom reference.[30] However, just like the spin-polarized (SP) curve in Fig. 1, the cohesive energy displays the well-known parabolic variation across the nonmagnetic transition-metal series.[31] On the other hand, the first-order pressure derivative of the bulk modulus varies almost linearly across the series.[32] In this paper the binding-energy curves have been calculated with respect to the non-spin-polarized free-atom state since we are not including any explicit magnetic contributions in the analytic expressions we consider. We will now use these DFT values of E_0, V_0, K_0, and K_0' to parametrize the binding-energy relations based on the Birch-Murnaghan, the extended Rydberg, and the generalized Morse expressions, respectively.

A. Birch-Murnaghan expansion

The Birch-Murnaghan expansion[6,7] expresses the energy of a bulk material as

$$E = -E_0\left[1 + \sum_{n>1} a^{(n)}\epsilon^n\right], \tag{1}$$

where ϵ is the Eulerian strain which is measured with respect to the strained state, namely,

$$\epsilon = [1-(V_0/V)^{2/3}]/2. \tag{2}$$

Writing $x=(V_0/V)^{1/3}$ and $V=V_0+\delta V$, we see that the above definition for strain reduces to the conventional linear strain $\epsilon=\delta x/x$ for $\epsilon \ll 1$. The form of Eq. (1) automatically satisfies the two equilibrium conditions that the binding energy at equilibrium equals $-E_0$ and the pressure vanishes at the equilibrium volume V_0 (since $a^{(1)}=0$). Three further parameters $a^{(2)}$, $a^{(3)}$, and $a^{(4)}$ may be fitted to K_0, K_0', and $E(\epsilon=1/2)=0$, which follows from the binding energy vanishing as the atoms are pulled apart to infinity.

The resultant *fourth-order* or *four-parameter* Birch-Murnaghan binding-energy relation is given by

$$E_{\rm bm} = -E_0\left(1 - \frac{9V_0K_0}{2E_0}[\epsilon^2 + (4-K_0')\epsilon^3 + 2\hat{a}_{\rm BER}^{(4)}\epsilon^4]\right), \tag{3}$$

where

$$\hat{a}_{\rm BER}^{(4)} = -\frac{a_{\rm BER}^{(4)}}{9V_0K_0/E_0} = K_0' + \frac{16E_0}{9V_0K_0} - 6. \tag{4}$$

The subscript BER is added to the quartic prefactor to remind us that the value is obtained by fitting the binding-energy relation to E_0, V_0, K_0 and K_0'. Interestingly we find the same combination of physical properties $E_0/(9V_0K_0)$ that defines the Rose scaling length l_r through[12]

$$\hat{l}_r = l_r/V_0^{1/3} = \sqrt{E_0/9V_0K_0}. \tag{5}$$

Therefore, if we follow Rose[12] and define a rescaled distance

$$x_r^* = (x-1)/\hat{l}_r = (V^{1/3}-V_0^{1/3})/l_r, \tag{6}$$

then Birch-Murnaghan equation (3) can be written in the normalized form,

$$E_{\rm bm}^*(x_r^*) = E_{\rm bm}/E_0 = -1 + (1/8\hat{l}_r^2)[1-(1+\hat{l}_r x_r^*)^{-2}]^2 + \cdots. \tag{7}$$

The plotting of the normalized Birch-Murnaghan binding energy against the rescaled Rose distance x_r^* has the advantage that all curves satisfy $E^*(0)=-1$, $E^{*\prime}(0)=0$, and $E^{*\prime\prime}(0)=1$, which can be verified by differentiating Eq. (7). This allows a ready comparison between the binding-energy curves of different metals across the transition-metal series.

Figure 2 compares the normalized analytic binding-energy relations to the DFT results for the $4d$ and $5d$ transition metals hcp Y and Lu, bcc Mo and W, and fcc Ag and Au. We see that whereas the fourth-order Birch-Murnaghan expression reproduces the binding-energy curves of the two noble metals extremely well, it fails under compression for the early and middle transition metals due to an instability. The occurrence of such an instability is not unexpected as Stacey,[15] Hofmeister,[16] and Holzapfel[17] pointed out that Eulerian strain (2) diverges as the volume shrinks so that the largest power in the truncated Birch-Murnaghan expression dominates. It follows from Eqs. (3) and (4) that if $\hat{a}_{\rm BER}^{(4)} = K_0' + 16E_0/(9V_0K_0) - 6$ is negative then the energy will behave anomalously. The plots in Fig. 3 of $\hat{a}_{\rm BER}^{(4)}$ across the $4d$

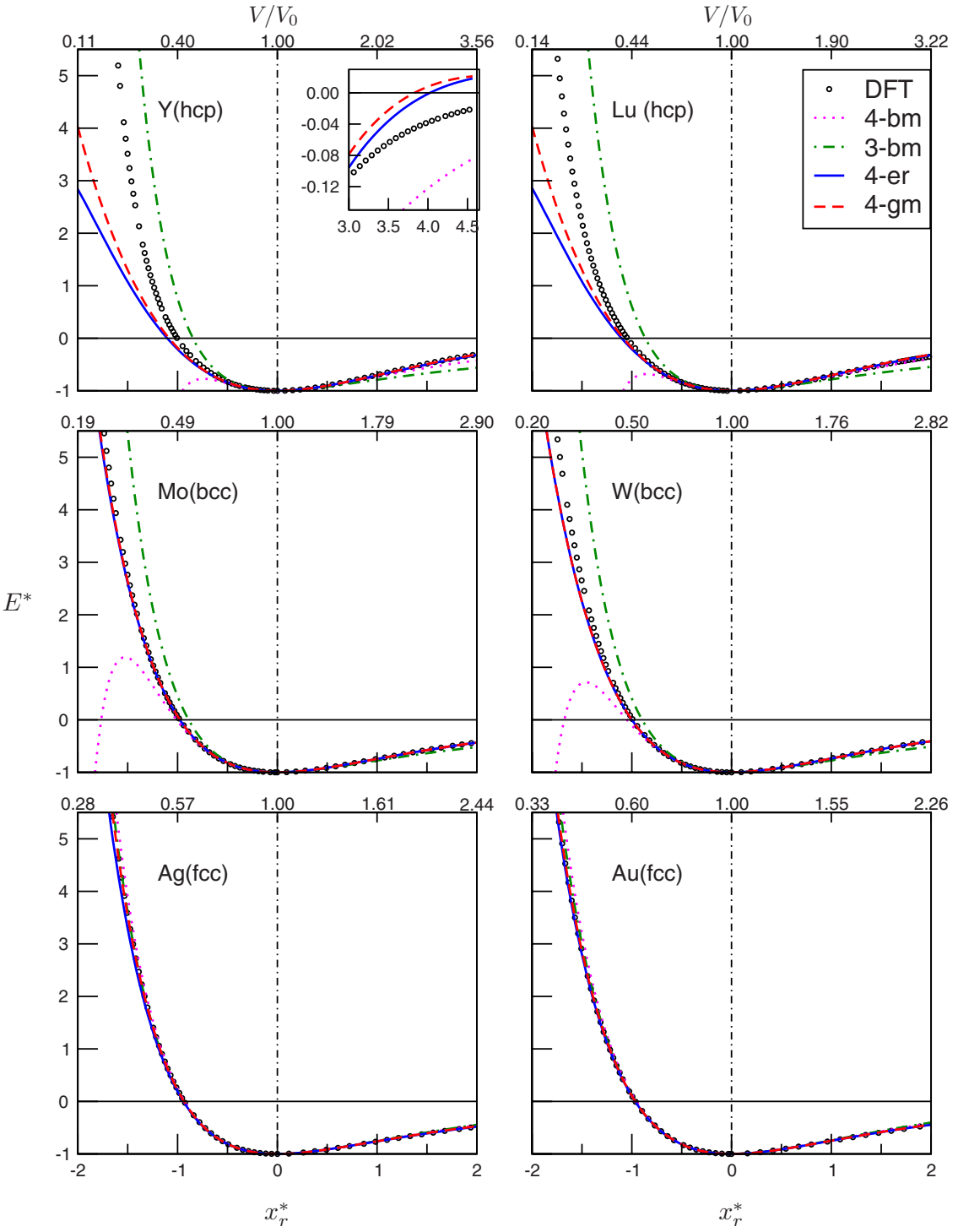

FIG. 2. (Color online) Normalized binding-energy curves for hcp Y and Lu, bcc Mo and W, and fcc Ag and Au. 4-bm: four-parameter Birch-Murnaghan expansion; 3-bm: three-parameter Birch-Murnaghan expansion; 4-er: four-parameter extended Rydberg expansion; 4-gm: four-parameter generalized Morse expression. In this figure, the 4-er and 4-gm cannot be visually distinguished for Mo, W, Ag, and Au, since their values are very close.

and $5d$ series confirm that an instability will occur in the fourth-order Birch-Murnaghan binding-energy relation for all non-noble transition metals.

This instability at fourth order can be avoided by working only to *third order* for which the Birch-Murnaghan binding energy takes the form,

$$E_{\rm bm} = -E_0\left\{1 - \frac{9V_0K_0}{2E_0}\left[\epsilon^2 - 2\left(1 - \frac{8E_0}{9V_0K_0}\right)\epsilon^3\right]\right\}. \quad (8)$$

For transition metals the prefactor of the cubic term, $[1-8E_0/(9V_0K_0)]$, is always positive since $\hat{l}_r = \sqrt{E_0/9V_0K_0}$ is

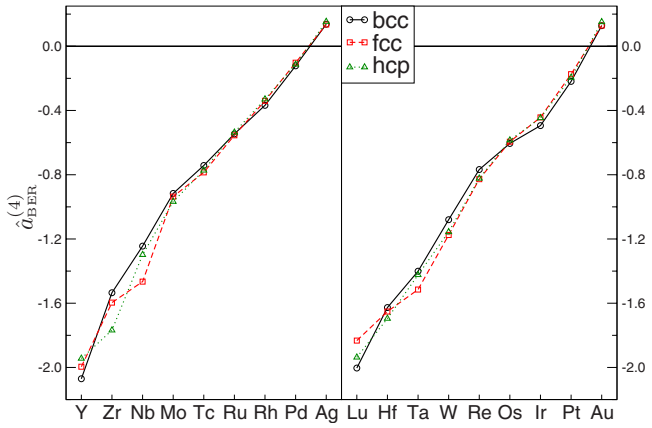

FIG. 3. (Color online) $\hat{a}^{(4)}_{\mathrm{BER}}$ in Birch-Murnaghan binding-energy relation across the 4*d* and 5*d* transition-metal series.

found to be less than $1/2\sqrt{2}$, so that Eq. (8) is well-behaved under compression. However, as can be seen from Fig. 2, the third-order expansion gives a very poor fit to the DFT values for Y, Lu, Mo, and W away from the immediate vicinity of equilibrium. Hence, the Birch-Murnaghan expansion does not give a good description of the binding-energy curves of the early and middle transition metals.

B. Extended Rydberg expansion

The extended Rydberg expansion[8,9] writes the energy of a bulk material as

$$E^*_{\mathrm{er}}(x^*) = E_{\mathrm{er}}/E_0 = -\left[1 + x^* + \sum_{n>1} c^{(n)}(x^*)^n\right]e^{-x^*}, \qquad (9)$$

where $x^* = (V^{1/3} - V_0^{1/3})/l$ is a measure of distance in terms of some scaling length l. The form of Eq. (9) automatically satisfies the two equilibrium conditions that $E^*(0) = -1$ and $E^{*\prime}(0) = 0$. The choice of the Rose scaling length from Eq. (5) guarantees that $E^{*\prime\prime}(0) = 1$. The additional fitting of $E^{*\prime\prime\prime}(0)$ or K_0' leads to the Rose binding-energy relation[12]

$$E^*_{\mathrm{er}}(x^*_r) = -[1 + x^*_r + c^{(3)}_{\mathrm{BER}}(x^*_r)^3]e^{-x^*_r}, \qquad (10)$$

where

$$c^{(3)}_{\mathrm{BER}} = \frac{1}{2}(K_0' - 1)\sqrt{\frac{E_0}{9V_0K_0}} - \frac{1}{3}. \qquad (11)$$

The original 1932 Rydberg potential for the dimer is analogous to this Rose equation for the bulk if we neglect the cubic contribution.

Figure 2 compares the normalized Rose binding-energy curves to the DFT results for the chosen 4*d* and 5*d* transition metals. We see that in addition to reproducing the noble metals well, the Rose form of the extended Rydberg expression also fits the group VI transition metals Mo and W well. However, the early transition metals Y and Lu are predicted to be too soft under compression as the observed hard-core repulsion is not reproduced.

C. Generalized Morse expression

The generalized Morse expression for the binding energy takes the exponential form,[10,11]

$$E_{\mathrm{gm}}(x) = Ae^{-p(x-1)} - Be^{-q(x-1)}, \qquad (12)$$

where the first contribution arises from the overlap repulsion and the second from the formation of covalent bonds (whether saturated as in *sp*-valent semiconductors or unsaturated as in *d*-valent transition metals).[31] The four parameters A, B, p, and q can be obtained by fitting to E_0, V_0, K_0, and K_0'. In particular, the *geometric mean* of the exponents of p and q is given by[36]

$$\sqrt{pq} = \sqrt{9V_0K_0/E_0} = V_0^{1/3}/l_r. \qquad (13)$$

The *arithmetic mean* of p and q is given by[22]

$$(p+q)/2 = 3(K_0' - 1)/2 = V_0^{1/3}/l_v. \qquad (14)$$

This scaling length l_v had previously been introduced by Vinet *et al.*[13] in his fitting of the extended Rydberg expansion to the equation of state (where V_0, K_0, and K_0' are known explicitly, but not E_0).

As pointed out in an earlier publication,[22] generalized Morse expression (12) can be rewritten in a form that appears not unlike the extended Rydberg expansion, namely,

$$E^*_{\mathrm{gm}}(x^*_v) = -[\sinh(\sqrt{\mu}x^*_v)/\sqrt{\mu} + \cosh(\sqrt{\mu}x^*_v)]e^{-x^*_v}, \qquad (15)$$

where

$$\mu = [(p-q)/(p+q)]^2 = 1 - [2\sqrt{pq}/(p+q)]^2. \qquad (16)$$

However, we see that the Vinet scaling length enters this expression rather than the Rose scaling length because the arithmetic mean $\frac{1}{2}(p+q)$ is the natural inverse scaling length for the generalized Morse expression with the sum of two exponentials. These two different scaling lengths, in fact, define the parameter μ since substituting Eqs. (13) and (14) into Eq. (16), we have

$$\mu_{\mathrm{BER}} = 1 - (l_v/l_r)^2. \qquad (17)$$

We have again added the subscript BER to stress that this expression is only valid when fitting binding-energy relations, since then the cohesive energy E_0 and hence the Rose scaling length l_r are calculated. Figure 4 shows that the variation in l_v and l_r across the 4*d* and 5*d* series, where we observe that $l_v > l_r$ for groups III, IV, and V, but $l_v < l_r$ otherwise. At the crossover point where $l_v = l_r$, we have $\mu_{\mathrm{BER}} = 0$, so that generalized Morse expression (15) reduces to the original Rydberg expression,

$$E^*_{\mathrm{er}}(x^*) = E_{\mathrm{er}}/E_0 = -[1 + x^*]e^{-x^*}, \qquad (18)$$

with $x^* = x^*_r = x^*_v$.

Figure 2 compares the normalized generalized Morse binding-energy curves to the DFT results for the chosen 4*d* and 5*d* transition metals. Not unexpectedly we see that the generalized Morse curves behave very similarly to the extended Rydberg case and fail to reproduce the observed hard-core repulsion of the early transition metals under compression. The extent of the failure may be quantified directly for

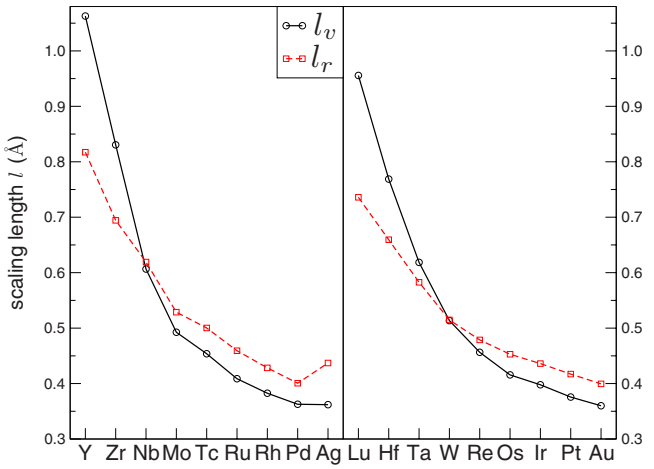

FIG. 4. (Color online) Trend of Rose and Vinet scaling lengths l_v and l_r, respectively, across the 4*d* and 5*d* transition-metal series. Ground-state structure is taken for each element.

the Morse curve by locating the points of the node x_{node} and point of inflection x_{infl} that satisfy $E(x_{\text{node}})=0$ and $E''(x_{\text{infl}})=0$, respectively. It follows from Eq. (12) that the generalized Morse expression predicts that they will be given by

$$1 - x_{\text{node}} = x_{\text{infl}} - 1 = \ln(p/q)/(p-q). \tag{19}$$

That is, the deviation between the DFT values on the left-hand side compared to the Morse values on the right-hand side is measured by

$$\delta_i = |1 - x_i| - \ln(p/q)/(p-q), \tag{20}$$

where i corresponds to either "node" or "inflection."

Figure 5 shows the deviation in the nodal point and point of inflection across the 4*d* and 5*d* transition-metal series. We see that the nodal point starts to deviate markedly as we proceed across to the left of the transition-metal series due to the increase in the size of the ion core providing additional hard-core repulsion.[31] However, comparing the 4*d* and 5*d* nodal curves, we find that whereas the deviation in the 4*d* curve continues to increase as we move from Nb→Zr→Y, the 5*d* curve displays instead a shallow minimum in going from Ta→Hf→Lu. It then increases dramatically across the lanthanide series from the Lu value of −0.01 to 1 order of magnitude larger value for La of −0.1. This reflects the lanthanide contraction due to the filling of 4*f* shell as we proceed from La to Lu, which results in their ionic core radii changing from 1.17 to 1.00 Å.[37] This lanthanide contraction has a noticeable influence on the properties of the early 5*d* transition-metal series[38] and is responsible for the shallow minimum in the nodal deviation in going from Ta→Hf→Lu. On the other hand, we see that apart from La the deviations in the point of inflection are relatively small across the 4*d* and 5*d* series. Thus, we find that the analytic expressions give a poor description of the binding-energy curves of the early transition metals Y and Lu in Fig. 2.

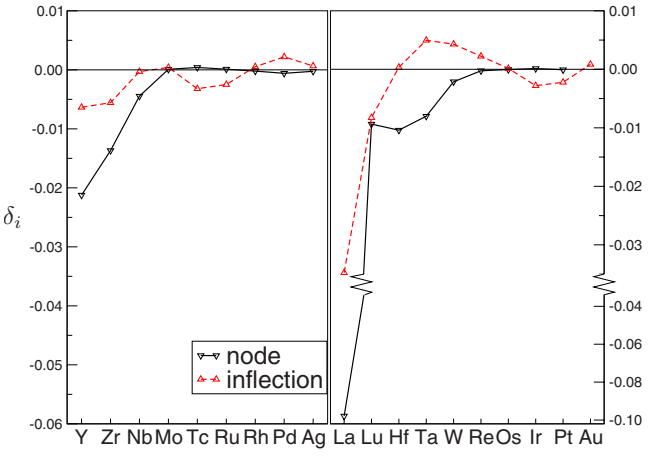

FIG. 5. (Color online) Deviation between the generalized Morse and DFT values of nodal point and point of inflection across the 4*d* and 5*d* transition-metal series. Ground-state structure is taken for each element.

The generalized Morse binding-energy curve for Y also displays an oscillation at large volume as can be seen in the inset of Fig. 2. This is a direct consequence of $l_v \geq l_r$ in Fig. 4 so that $\mu_{\text{BER}}<0$ with the consequence that $\sqrt{\mu_{\text{BER}}}$ is imaginary in the argument of the hyperbolic functions in Eq. (15). Thus the logical basis of the analytic Morse expression is lost because p and q will be complex and we can no longer separate the terms in Eq. (15) into real repulsive and attractive contributions as implied by Eq. (12).

The origin of this spurious oscillatory behavior appears to be related to the $s \rightarrow d$ electron transfer that takes place in transition metals under compression as the bottom of the valence *sp* band is pushed up through the *d* band by core orthogonality constraints.[39] This transfer will, of course, severely modify the behavior of the binding-energy relation[40,41] and corresponding equation of state.[42–45] For the early transition metals, the four-parameter generalized Morse expression with real values of p and q is unable to reproduce simultaneously the values of V_0, K_0, and K_0' *at equilibrium* and E_0, which depends on the total area under the equation of state as the atoms are brought together *from infinity*. The bonding contribution in Eq. (12) displays a simple exponential dependence that reflects the variation in the DFT *d*-band width under compression.[31] However, the prefactor B in Eq. (12) is treated as a constant whereas in practice it should be dependent on the *d*-band occupancy.[31] The DFT values of the logarithmic volume derivative of the number of valence *d*-electrons N_d at equilibrium are displayed in the right-hand panel of Fig. 6 for the 5*d* transition-metal series. We see that they reflect a similar trend across the series as the variation in μ_{BER} in the left-hand panel. A corresponding plot of the μ_{BER} and N_d derivative curves across the 4*d* transition-metal series was given earlier in Fig. 1 of Ref. 22.

III. EQUATIONS OF STATE

The failures of these analytic expressions to reproduce the binding-energy curves of the early transition metals are not surprisingly also displayed in the behavior of their equations of states. Whereas the binding-energy relations were fitted to V_0, K_0, K_0', and the cohesive energy E_0, the equations of state were fitted to V_0, K_0, K_0', and the second pressure derivative

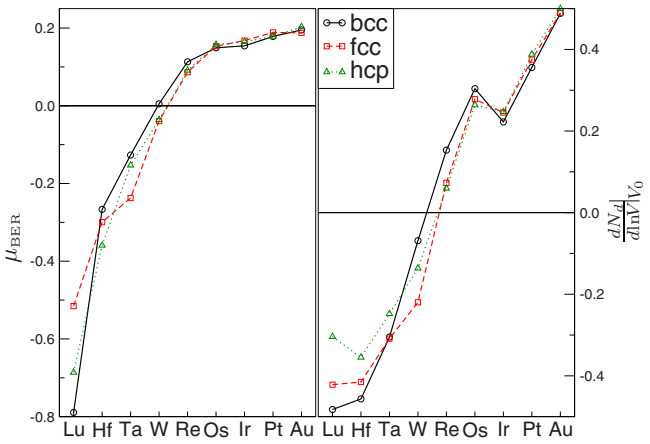

FIG. 6. (Color online) Trend of μ_{BER} and logarithmic volume derivative of number of valence d electrons at equilibrium across the 5d transition-metal series.

of the bulk modulus at equilibrium K_0''. Both K_0' and K_0'' are subject to more noise[46] in fitting the DFT data to a polynomial about equilibrium than V_0 and K_0 since they involve the third and fourth derivatives of the energy, respectively. In this paper, therefore, we have calculated them (and higher-order derivatives) using the procedure described in Ref. 22 and discussed later in Sec. IV.

A. Birch-Murnaghan expansion

The four-parameter Birch-Murnaghan equation of state[6,7,47] is given by

$$P = -\frac{3K_0}{x^5}\epsilon\left[1 - \frac{3}{2}(K_0' - 4)\epsilon + 4\hat{a}_{\mathrm{EOS}}^{(4)}\epsilon^2\right], \tag{21}$$

where

$$\hat{a}_{\mathrm{EOS}}^{(4)} = \frac{-a_{\mathrm{EOS}}^{(4)}[287 - 87K_0' + 9(K_0')^2 + 9K_0K_0'']}{384}$$
$$= \frac{3}{8}\left[K_0K_0'' + K_0'(K_0' - 7) + \frac{143}{9}\right]. \tag{22}$$

The subscript EOS is added to the quartic prefactor $\hat{a}_{\mathrm{EOS}}^{(4)}$ in the energy expression of Eq. (1) to remind us that it is obtained by fitting to the equation of state parameters V_0, K_0, K_0', and K_0'' and $\hat{a}_{\mathrm{EOS}}^{(4)}$ is plotted in Fig. 7 across the 4d and 5d transition-metal series. If we integrate this equation of state [Eq. (21)] from the equilibrium value V_0 out to infinity, then the predicted cohesive energy is given by

$$E_0^{\mathrm{pred}} = \frac{9}{16}K_0V_0(6 + \hat{a}_{\mathrm{EOS}}^{(4)} - K_0'). \tag{23}$$

Just as the most convenient way for comparing binding-energy curves of different transition metals is to plot the normalized energy E/E_0 versus the Rose scaled distance x_r^*, the equations of state are best compared by plotting the logarithm of the normalized Vinet function H^* versus the Vinet scaled distance x_v^*. The latter two coordinates are defined by

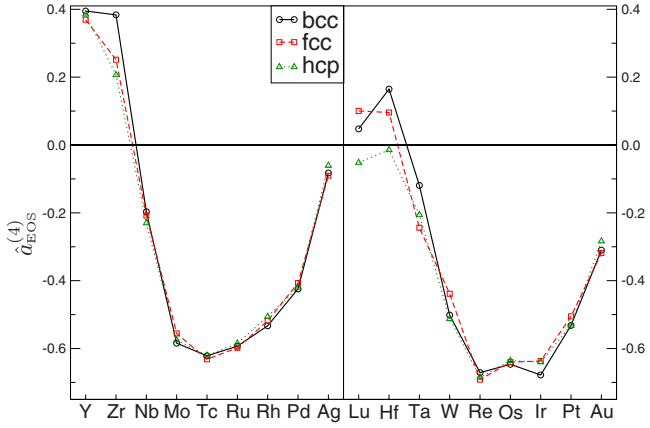

FIG. 7. (Color online) $\hat{a}_{\mathrm{EOS}}^{(4)}$ in Birch-Murnaghan equation of state across the 4d and 5d transition-metal series.

$$H^* = H/K_0 = Px^2/[3K_0(1 - x)], \tag{24}$$

and

$$x_v^* = (x - 1)/\hat{l}_v = (V^{1/3} - V_0^{1/3})/l_v \tag{25}$$

with $l_v = V_0^{1/3}/[3/2(K_0' - 1)]$ from Eq. (14). Vinet *et al.*[13] showed that using these two definitions

$$\ln H^* = -x_v^*, \tag{26}$$

to lowest order. This "universal" relation about equilibrium is clearly satisfied by the Birch-Murnaghan equation of state, since substituting ϵ from Eq. (2) into Eq. (21) leads to $H^*(0) = 1$ and $(\ln H^*)'(0) = -1$ at $x_v^* = 0$.

Figure 8 compares the normalized analytic equations of state to the DFT results for the chosen 4d and 5d transition metals. We see that whereas the four-parameter Birch-Murnaghan expansion reproduces the equation of state of the two noble metals under compression, it fails badly for Lu, Mo, and W due to the prefactor $\hat{a}_{\mathrm{EOS}}^{(4)}$ taking negative values for most transition metals, as can be seen in Fig. 7. On the other hand, the three-parameter expansion with $\hat{a}_{\mathrm{EOS}}^{(4)}$ taken as zero performs more robustly as it only fails for the early transition metals Y and Lu where $K_0' < 4$ (see Fig. 1).[16] This most probably accounts for the extensive use of the third order but not fourth-order Birch-Murnaghan equation of state in the literature. However, we should note that the predicted values of the cohesive energy, which are given in Table I, are generally in poor agreement with the non-spin-polarized DFT values.

B. Extended Rydberg expansion

It follows from Eq. (9) that the four-parameter extended Rydberg equation of state is given by

$$P = \frac{3K_0(1 - x)}{x^2}[1 + \hat{c}_{\mathrm{EOS}}^{(2)}(x_v^*)^2 + \hat{c}_{\mathrm{EOS}}^{(3)}(x_v^*)^3]e^{-x_v^*}, \tag{27}$$

where

$$\hat{c}_{\mathrm{EOS}}^{(2)} = 8/[3(1 - K_0')], \tag{28}$$

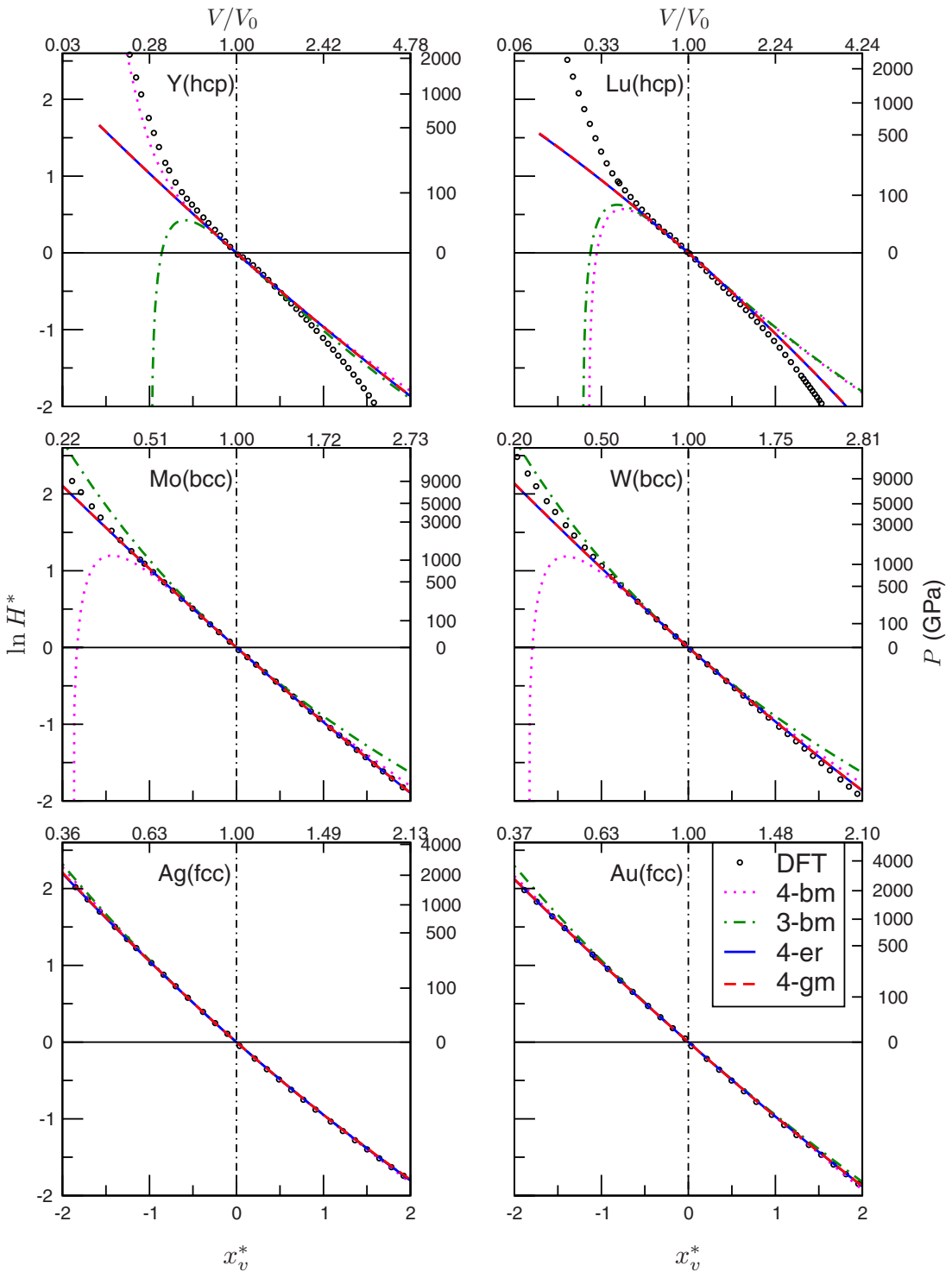

FIG. 8. (Color online) $\ln H^*$ plots for hcp Y and Lu, bcc Mo and W, and fcc Ag and Au. 4-bm: four-parameter Birch-Murnaghan expansion; 3-bm: three-parameter Birch-Murnaghan expansion; 4-er: four-parameter extended Rydberg expansion; 4-gm: four-parameter generalized Morse expression. In this figure, the 4-er and 4-gm cannot be visually distinguished since their values are very close.

$$\hat{c}_{\mathrm{EOS}}^{(3)} = \frac{125 + 18K_0' + 9(K_0')^2 + 36K_0K_0''}{54(1-K_0')^2}. \tag{29}$$

The predicted cohesive energy is given by

$$E_0^{\mathrm{pred}} = \frac{8V_0K_0[18K_0K_0'' + 9(K_0')^2]}{9(K_0'-1)^4}. \tag{30}$$

To lowest order, Eq. (27) immediately implies Vinet "universal" relation (26). We see that all the corresponding $\ln H^*$

TABLE I. Cohesive energy E_0^{pred} (eV) predicted from different analytic equations of state.

		DFT	4-bm	3-bm	4-er	4-gm
4*d*	Y (hcp)	5.10	15.84	14.06	10.48	10.98
	Mo (bcc)	11.57	16.86	26.16	11.70	12.03
	Ag (fcc)	3.76	1.98	2.69	3.41	3.82
5*d*	Lu (hcp)	4.44	13.64	13.90	5.18	5.72
	W (bcc)	12.59	23.28	32.54	15.21	15.93
	Au (fcc)	4.41	−0.65	2.96	4.27	4.43

plots in Fig. 8 are well behaved in that there are no singularities as found for some of the Birch-Murnaghan equations of state under compression. However, it is clear that the $\ln H^*$ plots do not display the hard-core repulsion at high pressures that is observed for Y, Lu, Mo, and W. In addition, the predicted value of the cohesive energy for Y is a factor of 2 too large.

C. Generalized Morse expression

As shown by Qin *et al.*,[22] the four-parameter generalized Morse expression for the normalized Vinet function H^* can be written in the compact form,

$$H^* = \frac{\sinh(\sqrt{\mu_{\text{EOS}}}x_v^*)}{\sqrt{\mu_{\text{EOS}}}x_v^*}e^{-x_v^*}, \tag{31}$$

where

$$\mu_{\text{EOS}} = \frac{4K_0K_0'' + (K_0')^2 + 2K_0' - \frac{19}{9}}{(K_0' - 1)^2}. \tag{32}$$

Thus, we recover the "universal" Vinet relation, in the limit as $\mu_{\text{EOS}} \to 0$. Integrating the equation of state out from equilibrium to infinity yields the predicted cohesive energy

$$E_0^{\text{pred}} = \frac{9K_0V_0}{7 - 9(K_0K_0'' + K_0')}. \tag{33}$$

As expected from an earlier discussion of the binding-energy curve in Fig. 2, we see in Fig. 8 that the four-parameter generalized Morse and extended Rydberg expressions behave very similarly over a wide range of pressures. In particular, they both fail to reproduce the hard-core contributions under compressions and the cohesive energies of the early transition metals.

TABLE II. Parameters of 6-pe expression for the 4*d* and 5*d* transition metals.

		A (eV)	*B* (eV)	*p*	*q*	*m*	*n*
4*d*	Y (hcp)	0.33	5.33	0.00	9.91	8.20	9.40
	Zr (hcp)	0.80	8.86	0.00	9.63	7.92	8.92
	Nb (bcc)	4.54	15.30	0.00	5.97	5.45	4.36
	Mo (bcc)	8.80	20.83	7.08	2.99	0.00	0.00
	Tc (hcp)	8.38	19.86	7.46	3.15	0.00	0.00
	Ru (hcp)	6.21	16.43	8.41	3.18	0.00	0.00
	Rh (fcc)	4.52	12.47	9.11	3.31	0.00	0.00
	Pd (fcc)	2.97	8.20	9.82	3.56	0.00	0.00
	Ag (fcc)	1.44	5.26	10.98	3.00	0.00	0.00
5*d*	Lu (hcp)	0.54	4.81	0.00	11.15	7.18	10.35
	Hf (hcp)	1.17	9.14	0.00	9.73	7.21	8.81
	Ta (bcc)	2.06	12.67	0.00	9.18	7.45	7.97
	W (bcc)	9.57	22.07	0.00	6.58	5.27	4.30
	Re (hcp)	12.91	26.06	7.14	3.54	0.00	0.00
	Os (hcp)	9.10	21.72	8.13	3.40	0.00	0.00
	Ir (fcc)	7.86	18.13	8.44	3.66	0.00	0.00
	Pt (fcc)	4.82	12.13	9.37	3.73	0.00	0.00
	Au (fcc)	2.85	7.28	10.22	4.00	0.00	0.00

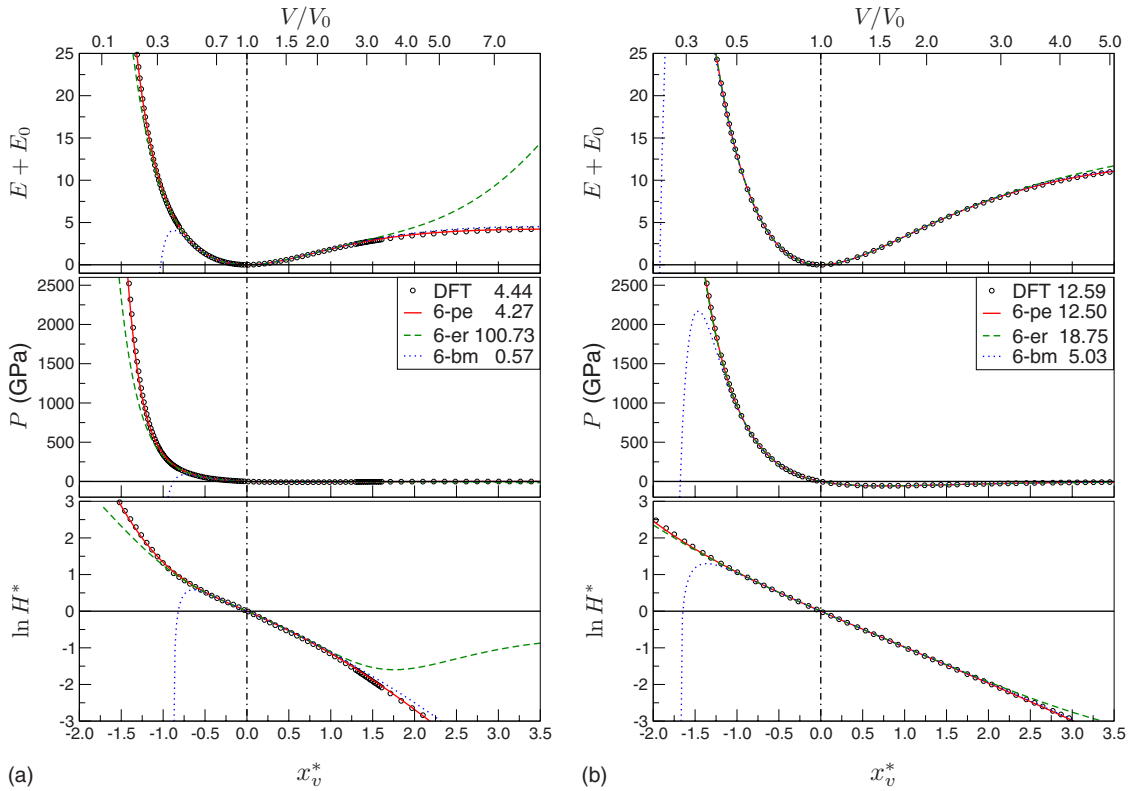

FIG. 9. (Color online) Shifted binding energy, pressure, and $\ln H^*$ plots for (a) hcp Lu and (b) bcc W. 6-pe: six-parameter power-exponential expression; 6-er: six-parameter extended Rydberg expansion; 6-bm: six-parameter Birch-Murnaghan expansion. Predicted cohesive energies E_0^{pred} obtained by integrating analytically equations of state are given (in eV) in insets of middle panels.

IV. MIXED POWER-EXPONENTIAL EXPRESSION

We have recently proposed a six-parameter analytic expression in an attempt to overcome the problems of lack of hard-core repulsion and poor cohesive energy prediction for the early transition metals.[22] It takes a mixed power-exponential form with the *binding-energy relation* being written as

$$E = A\frac{e^{-p(x-1)}}{x^m} - Bx^n e^{-q(x-1)} \tag{34}$$

with $m,n \geq 0$. We see that exponential generalized Morse expression (12) has been modified to include a divergent power-law prefactor in the repulsive contribution to model the hard-core repulsion, but a nondivergent power-law prefactor in the attractive term to provide an additional degree of freedom for fitting the binding-energy curve as the atoms are pulled apart to infinity.

We have obtained the six parameters A, B, p, q, m, and n as follows. First, A and B can be written down explicitly in terms of the equilibrium volume V_0 and bulk modulus K_0 as

$$A = 9K_0V_0(q-n)/C, \tag{35}$$

$$B = 9K_0V_0(p+m)/C, \tag{36}$$

with

$$C = (p+m)(q-n)[(p+m)-(q-n)] + (pn+qm). \tag{37}$$

This results in an *equation of state* that depends on V_0, K_0, and the remaining four parameters p, q, m, and n, namely,

$$P = \frac{3K_0}{x^2C}[(p+m/x)(q-n)x^{-m}e^{-p(x-1)} - (p+m)(q-n/x)x^n e^{-q(x-1)}]. \tag{38}$$

In this paper, we have fitted the parameters to the DFT pressure data over the range from 1000 GPa to $7V_0$. The upper pressure value of 1000 GPa has been chosen since it represents the current experimental limit that can be reached in a laboratory.[17,48] The corresponding values of A, B, p, q, m, and n are given in Table II across the $4d$ and $5d$ transition-metal series. Importantly, we see that this six-parameter power-exponential (6-pe) expression reduces to the four-parameter generalized Morse (4-gm) expression for all but the early transition metals Y, Zr, Nb and Lu, Hf, Ta, and W, since all the other elements are found to be optimally fitted for $m=0$ and $n=0$. This is not surprising since an inspection of the deviation between the 4-gm and DFT plots of $\ln H^*$ versus x_v^* reveals that only these early transition metals display noticeable signs of any deviation for $P<1000$ GPa. If we set a critical pressure to correspond to the deviation $[\ln H^*(\text{DFT}) - \ln H^*(\text{4-gm}) = 0.02]$, then the $4d$ elements Y, Zr, Nb, Mo, and Tc have the critical pressures 15, 108, 457, 2007, and 6592 GPa, respectively; whereas the $5d$ elements Lu, Hf, Ta, W, and Re have the values 46, 96, 290, 783, and 1242 GPa, respectively. Thus, for pressures less than 1000

TABLE III. Equilibrium properties obtained from 6-pe expression for the 4*d* and 5*d* transition metals.

		V_0 (Å^3)	K_0 (GPa)	K_0'	$K_0'' \times 10$ (GPa^{-1})	$K_0''' \times 10^3$ (GPa^{-2})	$K_0^{\mathrm{IV}} \times 10^3$ (GPa^{-3})	E_0^{pred} (6-pe) (eV)	E_0 (DFT) (eV)
4*d*	Y (hcp)	30.0	44	2.95	−0.64	11.97	−2.78	5.00	5.10
	Zr (hcp)	22.0	106	3.25	−0.29	2.53	−0.30	8.06	8.05
	Nb (bcc)	17.1	194	3.83	−0.23	0.99	−0.07	10.75	10.76
	Mo (bcc)	15.2	297	4.36	−0.21	0.68	−0.04	12.03	11.57
	Tc (hcp)	13.9	344	4.54	−0.19	0.50	−0.02	11.48	11.65
	Ru (hcp)	13.3	366	4.86	−0.19	0.52	−0.02	10.22	10.27
	Rh (fcc)	13.4	318	5.14	−0.24	0.78	−0.04	7.94	7.78
	Pd (fcc)	14.3	228	5.46	−0.38	1.80	−0.15	5.22	4.98
	Ag (fcc)	16.2	138	5.66	−0.62	4.97	−0.69	3.82	3.76
5*d*	Lu (hcp)	29.5	47	3.16	−0.80	15.51	−4.17	4.27	4.44
	Hf (hcp)	20.8	122	3.38	−0.29	2.19	−0.23	7.96	8.17
	Ta (bcc)	17.3	219	3.79	−0.20	0.83	−0.05	10.61	10.78
	W (bcc)	15.5	339	4.24	−0.17	0.47	−0.02	12.50	12.59
	Re (hcp)	14.5	409	4.56	−0.16	0.37	−0.01	13.15	12.82
	Os (hcp)	13.8	451	4.84	−0.16	0.35	−0.01	12.62	12.46
	Ir (fcc)	13.9	405	5.03	−0.19	0.47	−0.02	10.27	10.41
	Pt (fcc)	14.9	305	5.37	−0.28	0.98	−0.06	7.31	7.33
	Au (fcc)	16.8	192	5.74	−0.49	2.93	−0.30	4.43	4.41

GPa all the transition metals to the right of Nb in the 4*d* series and W in the 5*d* series will not be sensitive to the divergent hard-core contribution.

Figure 9 compares the six-parameter analytic binding energy, pressure, and ln H^* curves with those of DFT for the 5*d* elements hcp Lu and bcc W. A similar plot for the 4*d* element Y has already been published elsewhere.[22] The 6-pe curves were fitted to the DFT pressure database as outlined above. The six-parameter Birch-Murnaghan and extended Rydberg curves were then obtained from the values of V_0, K_0 and the analytic derivatives of K_0', K_0'', K_0''', and K_0^{IV} that correspond to the fitted 6-pe curve. They are given explicitly in Table III using the values of A, B, p, q, m, and n listed in Table II.

We see in Fig. 9 that the 6-pe equation of state and ln H^* plots fit both the high pressure and the large volume regions extremely well. On the other hand, the six-parameter Birch-Murnaghan equation of state and ln H^* curves show divergences under compression that we had found earlier with the four-parameter Birch-Murnaghan plots. The six-parameter extended Rydberg expansion also fails to reproduce the hard-core behavior of the Lu curves but performs well for W. Both the Birch-Murnaghan and extended Rydberg values for the predicted cohesive energies are extremely bad; whereas the 6-pe predicted values across the 4*d* and 5*d* series are in excellent agreement with the non-spin-polarized DFT results, as can be observed in Table III.

It is appropriate to comment here on the asymptotic behavior of K'. Several authors[5,49] have noted that the exponential form of the Morse and Rydberg expressions will lead to $K_\infty' = 2/3$; whereas experimentally the earth's inner core that consists of mainly iron, for example, appears to take the infinite pressure asymptote of $K_\infty' = 3.0 \pm 0.1$.[50] In Fig. 10, we have plotted the variation in K' from zero pressure up to 3000 GPa using the analytic 6-pe equation of state in Fig. 9 for Lu and W and the analytic 4-gm equation of state in Fig. 8 for Au. We see that Lu and W with their power-law repulsion and corresponding asymptote $K_\infty' = 1 + m/3$ reach their asymptotic values of 3.39 and 2.75 very quickly, whereas Au with its exponential behavior is very far from its theoretical asymptotic value of 2/3. In fact, Au takes a value of $K' = 2.95$ at 3000 GPa that is close to the "asymptotic" value of iron. We conclude, therefore, that the exponential extended Rydberg and generalized Morse expressions perform well for those metals (such as the later transition metals) in which the hard-core region has not yet been reached by experimental conditions.

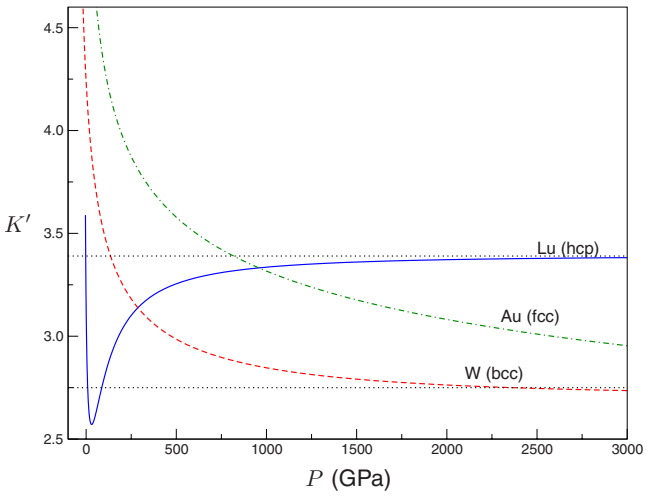

FIG. 10. (Color online) Variation in K' against pressure obtained from 6-pe expression. Asymptotic values for Lu and W of 3.39 and 2.75, respectively, are shown by horizontal dotted lines.

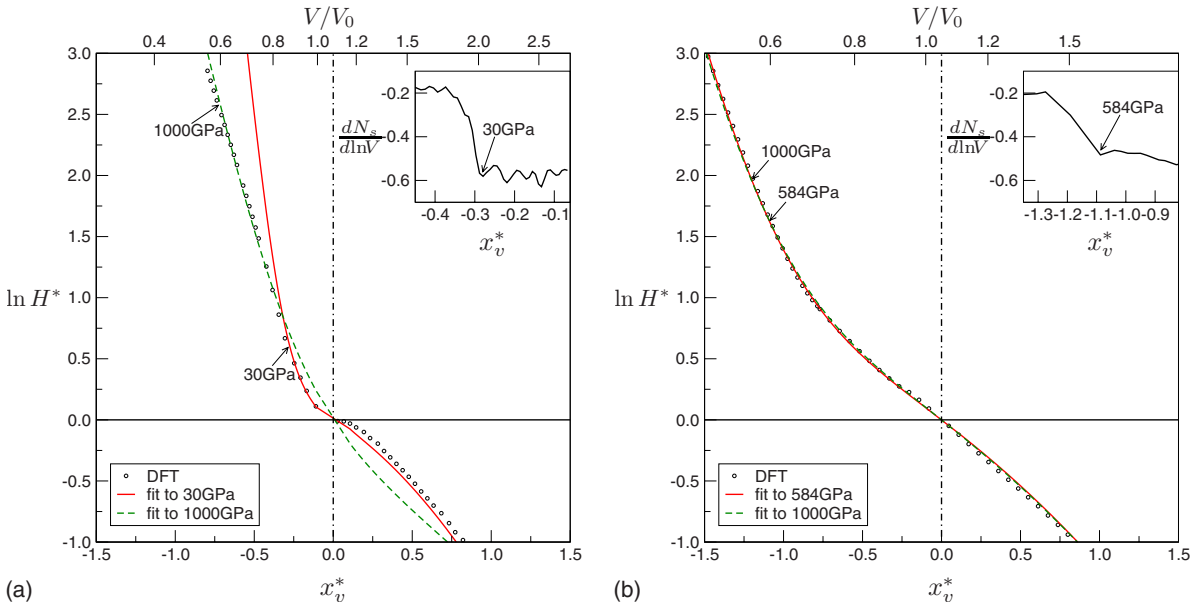

FIG. 11. (Color online) ln H^* plots for (a) hcp La and (b) hcp Lu with 6-pe parameters fitted to DFT values over a range of 1000 GPa to $7V_0$ (dashed curves) and also 30 GPa to $7V_0$ (full curve) for La and 584 GPa to $7V_0$ (full curve) for Lu. Insets show the logarithmic volume derivative of the number of valence s electrons N_s versus Vinet scaling length.

Finally, as a caveat we stress that not all transition metals have their equations of state well described by the 6-pe expression. The left-hand panel of Fig. 11 shows the ln H^* plot for hcp La where we see that the 6-pe fit between 1000 GPa and $7V_0$ fails to reproduce the slope of the DFT curve about the origin. This anomalous behavior was analyzed in detail by McMahan *et al.*[44] using the Pettifor-Andersen expression for the s, p, d, and f partial pressures.[39,43,51] They found that the anomaly is directly related to the valence s to d electron transfer that is expected for the early transition metals under pressure.[31] This is seen in the inset of the left-hand panel of Fig. 11, which displays the variation in the logarithmic volume derivative of the number of s electrons as we pass through equilibrium. Initially for La, at positive values of x_v^* this takes a fairly constant negative value of −0.6 corresponding to the valence 6s electrons being lost to the valence 5d (and 4f) bands under compression. This results in a net softening of the pressure due to additional bonding states being filled, which is reflected in the downward curvature of the ln H^* plot in this region. However, for negative values of x_v^* as the bottom of the 6s band approaches and moves up through the Fermi level, this 6s pool of valence electrons is lost to the system, resulting in an abrupt ending of the softening and the observed stiffening of the pressure curve.[44] We see in the left-hand panel of Fig. 11 that fitting the DFT data for La up to a pressure of 30 GPa at which the transition is observed shown in its inset leads to a 6-pe curve that reproduces the DFT values extremely well up to the transition but fails above it. On the other hand, this transition occurs in Lu at the much higher pressure of 584 GPa due to the lanthanide contraction, as can be seen in the right-hand panel of Fig. 11. The anomalous behavior that is observed around equilibrium for La is thus hidden in Lu due to its occurrence at higher pressures. A similar but weaker anomaly is also observed for the 3d element Sc.

V. CONCLUSION

We have examined in details the successes and failures of the Birch-Murnaghan, extended Rydberg, and generalized Morse binding-energy relations and equations of state for the 4d and 5d transition metals by comparing these analytic expressions to the corresponding first-principles DFT curves. As expected, all these analytic expressions were found to reproduce well the DFT binding-energy curves and equations of state for the late transition metals. However, for most early and middle transition metals, the fourth-order Birch-Murnaghan expression was observed to behave anomalously under compression due to divergences. This resulted in either negative energy or pressure values. The four-parameter extended Rydberg and generalized Morse expressions, on the other hand, did not behave abnormally but failed to reproduce the observed hard-core repulsion of the early transition metals under compression. In addition, the four-parameter extended Rydberg and generalized Morse binding-energy curves were found to oscillate under expansion in order to satisfy simultaneously the DFT values of the cohesive energy E_0 (equivalent to integrating the equation of state from equilibrium out to infinity) and the DFT values of the bulk modulus K_0 and pressure derivative K_0' at the equilibrium volume V_0.

These failures of the four-parameter Birch-Murnaghan, extended Rydberg, and generalized Morse expressions were then shown to be removed by using a recently proposed six-parameter mixed power-exponential expression. In particular, this six-parameter expression not only reproduced the observed hard-core repulsion under compression but also removed the spurious oscillations that had been predicted for the early 4d and 5d transition metals under expansion. On the other hand, the six-parameter Birch-Murnaghan and extended Rydberg expressions still behaved poorly with the

Birch-Murnaghan remaining anomalous under compression and the extended Rydberg deviating badly from the DFT curves under expansion. In conclusion, however, we must stress that this analytic six-parameter expression is not applicable to all metals as it is unable to reproduce, for example, the well-known anomalous behavior of the equation of state of La at the beginning of the $4f$ lanthanide series.

ACKNOWLEDGMENT

T.Q. would like to thank the EPSRC-GB for financial support under Grant No. GR S81155/01.

*ting.qin@materials.ox.ac.uk

[1] S. M. Foiles, M. I. Baskes, and M. S. Daw, Phys. Rev. B **33**, 7983 (1986).
[2] X. D. Dai, Y. Kong, and J. H. Li, Phys. Rev. B **75**, 104101 (2007).
[3] C. Bercegeay, G. Jomard, and S. Bernard, Phys. Rev. B **77**, 104203 (2008).
[4] G. J. Ackland and R. Thetford, Philos. Mag. A **56**, 15 (1987).
[5] F. D. Stacey, Rep. Prog. Phys. **68**, 341 (2005).
[6] F. Birch, J. Geophys. Res. **57**, 227 (1952).
[7] F. D. Murnaghan, *Finite Deformation of an Elastic Solid* (Dover, New York, 1951).
[8] R. Rydberg, Z. Phys. **73**, 376 (1932).
[9] P. Huxley and J. Murrell, J. Chem. Soc., Faraday Trans. 2 **79**, 323 (1983).
[10] P. M. Morse, Phys. Rev. **34**, 57 (1929).
[11] F. Ducastelle, J. Phys. (France) **31**, 1055 (1970).
[12] J. H. Rose, J. R. Smith, F. Guinea, and J. Ferrante, Phys. Rev. B **29**, 2963 (1984).
[13] P. Vinet, J. Ferrante, J. R. Smith, and J. H. Rose, J. Phys. C **19**, L467 (1986).
[14] J. C. Slater, *Introduction to Chemical Physics* (McGraw-Hill, New York, London, 1939).
[15] F. D. Stacey, B. J. Brennan, and R. D. Irvine, Geophys. Surv. **4**, 189 (1981).
[16] A. M. Hofmeister, Geophys. Res. Lett. **20**, 635 (1993).
[17] W. B. Holzapfel, Rep. Prog. Phys. **59**, 29 (1996).
[18] R. Jeanloz, Phys. Rev. B **38**, 805 (1988).
[19] S. K. Sikka, Phys. Rev. B **38**, 8463 (1988).
[20] P. Vinet, J. H. Rose, J. Ferrante, and J. R. Smith, J. Phys.: Condens. Matter **1**, 1941 (1989).
[21] A. T. Paxton, M. Methfessel, and H. M. Polatoglou, Phys. Rev. B **41**, 8127 (1990).
[22] T. Qin, R. Drautz, and D. G. Pettifor, Phys. Rev. B **77**, 220103(R) (2008).
[23] G. Kresse and J. Furthmüller, Phys. Rev. B **54**, 11169 (1996).
[24] G. Kresse and J. Furthmüller, Comput. Mater. Sci. **6**, 15 (1996).
[25] P. E. Blöchl, Phys. Rev. B **50**, 17953 (1994).
[26] D. M. Ceperley and B. J. Alder, Phys. Rev. Lett. **45**, 566 (1980).
[27] J. P. Perdew, K. Burke, and M. Ernzerhof, Phys. Rev. Lett. **77**, 3865 (1996).
[28] G. Kresse and D. Joubert, Phys. Rev. B **59**, 1758 (1999).
[29] H. J. Monkhorst and J. D. Pack, Phys. Rev. B **13**, 5188 (1976).
[30] E. G. Moroni, G. Kresse, J. Hafner, and J. Furthmüller, Phys. Rev. B **56**, 15629 (1997).
[31] D. G. Pettifor, *Bonding and Structure of Molecules and Solids* (Oxford University Press, Oxford, 1995).
[32] D. J. Steinberg, J. Phys. Chem. Solids **43**, 1173 (1982).
[33] C. Kittel, *Introduction to Solid State Physics*, 8th ed. (Wiley, New York, 2005).
[34] R. Jeanloz, B. K. Godwal, and C. Meade, Nature (London) **349**, 687 (1991).
[35] G. N. Chesnut and Y. K. Vohra, Phys. Rev. B **57**, 10221 (1998).
[36] D. Spanjaard and M. C. Desjonquères, Phys. Rev. B **30**, 4822 (1984).
[37] R. Shannon, Acta Crystallogr., Sect. A: Cryst. Phys., Diffr., Theor. Gen. Crystallogr. **32**, 751 (1976).
[38] D. G. Pettifor, Mater. Sci. Technol. **4**, 2480 (1988).
[39] D. G. Pettifor, J. Phys. F: Met. Phys. **7**, 613 (1977).
[40] J. C. Duthie and D. G. Pettifor, Phys. Rev. Lett. **38**, 564 (1977).
[41] J. A. Moriarty, Phys. Rev. B **45**, 2004 (1992).
[42] D. G. Pettifor, Commun. Phys. (London) **1**, 141 (1976).
[43] D. G. Pettifor, J. Phys. F: Met. Phys. **8**, 219 (1978).
[44] A. K. McMahan, H. L. Skriver, and B. Johansson, Phys. Rev. B **23**, 5016 (1981).
[45] Y. K. Vohra, S. K. Sikka, and W. B. Holzapfel, J. Phys. F: Met. Phys. **13**, L107 (1983).
[46] O. L. Anderson, *Equations of State of Solids for Geophysics and Ceramic Science* (Oxford University Press, Oxford, 1995).
[47] F. Birch, J. Phys. Chem. Solids **38**, 175 (1977).
[48] A. E. Gheribi, J.-M. Roussel, and J. Rogez, J. Phys.: Condens. Matter **19**, 476218 (2007).
[49] W. B. Holzapfel, High Press. Res. **16**, 81 (1998).
[50] F. D. Stacey and P. M. Davis, Phys. Earth Planet. Inter. **142**, 137 (2004).
[51] O. K. Andersen, Phys. Rev. B **12**, 3060 (1975).